

Communication

**Aromatic extension at 2,6- positions of anthracene towards
an elegant strategy for organic semiconductors with
efficient charge transport and strong solid state emission**

Jie Li, Ke Zhou, Jie Liu, Yonggang Zhen, Li Liu, Jidong Zhang,
Huanli Dong, Xiaotao Zhang, Lang Jiang, and Wenping Hu

J. Am. Chem. Soc., **Just Accepted Manuscript** • DOI: 10.1021/jacs.7b09381 • Publication Date (Web): 07 Nov 2017

Downloaded from <http://pubs.acs.org> on November 7, 2017

Just Accepted

“Just Accepted” manuscripts have been peer-reviewed and accepted for publication. They are posted online prior to technical editing, formatting for publication and author proofing. The American Chemical Society provides “Just Accepted” as a free service to the research community to expedite the dissemination of scientific material as soon as possible after acceptance. “Just Accepted” manuscripts appear in full in PDF format accompanied by an HTML abstract. “Just Accepted” manuscripts have been fully peer reviewed, but should not be considered the official version of record. They are accessible to all readers and citable by the Digital Object Identifier (DOI®). “Just Accepted” is an optional service offered to authors. Therefore, the “Just Accepted” Web site may not include all articles that will be published in the journal. After a manuscript is technically edited and formatted, it will be removed from the “Just Accepted” Web site and published as an ASAP article. Note that technical editing may introduce minor changes to the manuscript text and/or graphics which could affect content, and all legal disclaimers and ethical guidelines that apply to the journal pertain. ACS cannot be held responsible for errors or consequences arising from the use of information contained in these “Just Accepted” manuscripts.

Aromatic extension at 2,6- positions of anthracene towards an elegant strategy for organic semiconductors with efficient charge transport and strong solid state emission

Jie Li,^{†,‡,§} Ke Zhou,^{†,‡,§} Jie Liu,[†] Yonggang Zhen,^{*,†} Li Liu,[§] Jidong Zhang,[§] Huanli Dong,^{*,†} Xiaotao Zhang,[†] Lang Jiang,[†] Wenping Hu^{*,†,†}

[†]Beijing National Laboratory for Molecular Science, Key Laboratory of Organic Solids, Institute of Chemistry, Chinese Academy of Sciences, Beijing 100190, China.

[†]Tianjin Key Laboratory of Molecular Optoelectronic Sciences, Department of Chemistry, School of Science, Tianjin University and Collaborative Innovation Center of Chemical Science and Engineering, Tianjin 300072, China

[‡]University of Chinese Academy of Sciences, Beijing 100190, China.

[§]State Key Laboratory of Polymer, Physics and Chemistry, Changchun Institute of Applied Chemistry, Chinese Academy of Sciences, Changchun, 130022, China

Supporting Information

ABSTRACT: Organic semiconductors integrating excellent charge transport with efficient solid emission are very challenging to be attained in the construction of light-emitting transistors and even for realization of electrically pumped organic lasers. Herein, we introduce naphthyl units at 2,6-positions of anthracene to achieve 2,6-di(2-naphthyl)anthracene (dNaAnt), which adopts J-aggregated mode in the solid state as a balanced strategy for excellent charge transporting and efficient solid state emission. Single crystal field-effect transistors (SC-FETs) show mobility up to $12.3 \text{ cm}^2 \cdot \text{V}^{-1} \cdot \text{s}^{-1}$ and a photoluminescence quantum yield (PLQY) of 29.2% was obtained for dNaAnt crystals. Furthermore, organic light-emitting transistors (OLETs) based on dNaAnt single crystals distribute outstanding balanced ambipolar charge transporting property ($\mu_h = 1.10 \text{ cm}^2 \cdot \text{V}^{-1} \cdot \text{s}^{-1}$, $\mu_e = 0.87 \text{ cm}^2 \cdot \text{V}^{-1} \cdot \text{s}^{-1}$) and spatially controllable emission, which is one of the best performances for OLETs.

Multifunctional organic semiconductors are highly pursued for the development of integrated optoelectronic devices, which is regarded as a gateway for a variety of applications.^{1,2} Particularly, OLETs, embodying the smallest possible integration of organic light emitting diodes (OLEDs) and field-effect transistors (OFETs), remarkably simplify the structure of active matrix displays.^{3,4} However, it remains a formidable task to design molecules combining high carrier mobility with efficient solid state emission since compact packing with strong and plentiful intermolecular interactions usually not only give rise to excellent charge transporting property but also quench terribly the solid state luminescence. This contradiction severely hinders the advancement of OLETs and the realization of electrically pumped organic lasers.³⁻⁶ For example, rubrene, with a single crystal mobility (μ_{SC}) about $15 \text{ cm}^2 \cdot \text{V}^{-1} \cdot \text{s}^{-1}$,⁷ has a photoluminescence quantum yield (PLQY) less than 1% in crystalline state. Though considerable efforts have been devoted to the design and synthesis of such kind materials, till now, very few molecular systems can compromise charge transporting and solid state emission.⁸⁻¹² Most of them suffer from either one or all of the following problems: (i)

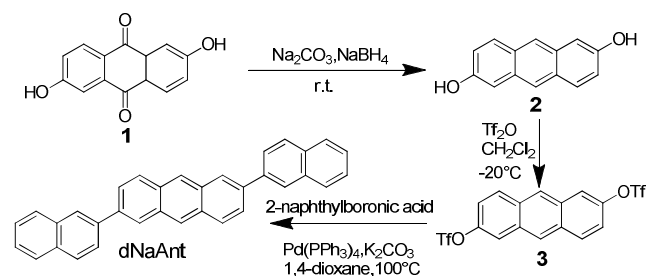
inefficient solid state emission;^{13,14} (ii) low charge carrier mobility;¹⁴⁻¹⁶ (iii) unmatched energy levels with the metal electrodes.¹⁷

Among the diverse molecular systems, anthracene, known as a highly luminescent molecule, has recently emerged as novel promising high performance organic emissive semiconductor. In 2012, Perepichka and coworkers reported the first anthracene based organic semiconductor with integrated high mobility and solid state emission, 2-(4-hexylphenylvinyl) anthracene (HPVAnt).⁸ Although reasonable hole mobility ($\mu_{\text{SC}} = 2.62 \text{ cm}^2 \cdot \text{V}^{-1} \cdot \text{s}^{-1}$) and high emission (PLQY = 70%) was achieved, the emission area mainly located in the vicinity of the electrode due to the unbalanced electron mobility in the channel, resulting from the mismatch of the energy levels of HPVAnt and the electrodes. In 2015, our group developed a highly emissive organic semiconductor, 2,6-diphenylanthracene (DPA), exhibiting a mobility up to $34 \text{ cm}^2 \cdot \text{V}^{-1} \cdot \text{s}^{-1}$ and a PLQY of 41.2% for crystals.¹¹ Unfortunately, DPA suffers from high threshold voltage due to the large offset between the energy levels of DPA and the electrodes. Here, we introduce naphthyl units into the 2,6- positions of anthracene to design a new anthracene derivative, 2,6-di(2-naphthyl)anthracene (dNaAnt) with the following considerations: (i) the substitution at the same sites as DPA and HPVAnt might maintain the J-aggregated mode and thus retain efficient emission; (ii) the introduction of naphthyl units into the anthracene core can prolong the conjugation length, which is expected to tune the energy levels and packing arrangements for the efficient charge injection and charge transport. Encouragingly, dNaAnt crystals adopt the J-aggregated mode, leading to a PLQY of 29.2%. Thanks to the prolonged conjugated length and compact packing motif, dNaAnt-based field-effect transistors show a single crystal mobility as high as $12.3 \text{ cm}^2 \cdot \text{V}^{-1} \cdot \text{s}^{-1}$. Furthermore, light-emitting transistors of dNaAnt single crystals demonstrate outstanding balanced ambipolarity: $\mu_h = 1.10 \text{ cm}^2 \cdot \text{V}^{-1} \cdot \text{s}^{-1}$, $\mu_e = 0.87 \text{ cm}^2 \cdot \text{V}^{-1} \cdot \text{s}^{-1}$, which is among the highest performances for OLETs. Conspicuous emission and obvious shift of the emission zone can be observed in OLETs, which can be attributed to efficient injection and transporting of charge carriers because of the suitable energy level alignment. These results make dNaAnt a promising candidate for

integrated optoelectronic applications and offer a facile strategy to the design and synthesis of such kind materials.

As described in scheme 1, dNaAnt was synthesized through three simple steps in a total yield of 40.5%. First, 2,6-dihydroxyanthraquinone (**1**) was reduced by sodium borohydride to give 2,6-dihydroxyanthracene (**2**), which further proceed the esterification reaction to afford 2,6-bis(trifluoromethanesulfonate)anthracene (**3**). Finally, dNaAnt was achieved by a Suzuki coupling and was further purified by sublimation for device fabrication.

Scheme 1. Synthetic route to dNaAnt



The absorption spectra of dNaAnt in THF solution show a well-structured vibrational band of typical anthracene derivatives peaking at $\lambda = 404, 384,$ and 365 nm (Figure 1a.), which corresponds to 0-0, 0-1 and 0-2 vibronic peak respectively. Compared with that of solution, the absorption of thin film and single crystals demonstrate an obvious bathochromic shift (33 nm) with peaks at 437 nm, 411 nm and 388 nm, indicating strong interactions between molecules in the solid state. The 0-0 peak of dNaAnt single crystals in the photoluminescence spectra (Figure 1b) appears at 452 nm, generating a Stokes shift of ~ 707.2 cm^{-1} , much smaller than that of solution (1055.8 cm^{-1}). This is probably because of the smaller configuration difference between the exciting state and the ground state for solid state than that for solution and less energy loss was obtained for the solid state. Bright blue-green emission can be observed from the dNaAnt crystals, as displayed in Figure 1c. The photoluminescence quantum yield of dNaAnt was 61.2% in solution and 29.2% for single crystals respectively. The red shift of the 0-0 absorption, the enhanced 0-0 vibronic peak intensity and the increased radiative decay rate ($K_f = \Phi_f/\tau$, Φ_f : the fluorescence quantum yield; τ : the fluorescence lifetime; Figure S1) suggest a J-aggregated mode of dNaAnt in solid state,^{18,19} which is thought to be the balanced strategy to achieve high mobility and efficient solid state emission coordinately. From the UV-Vis absorption spectra in crystal state, the energy gap was calculated to be 2.73 eV. The highest unoccupied molecular orbital level (HOMO) and lowest unoccupied molecular orbital (LUMO) level estimated from ultraviolet photoelectron spectroscopy (UPS, Figure S2) and energy gap was -5.33 eV, -2.60 eV respectively, corresponding well with cyclic voltammetry (CV) results (Figure S3). The HOMO energy level of dNaAnt is about 0.3 or 0.17 eV higher than that of DPA or HPVAnt respectively (Figure S4), ensuring better match with Fermi energy level of the gold electrode. DFT calculations were further performed to shed insights into the frontier molecular orbitals distribution (Figure 1d). π -electron densities of HOMO and LUMO distribute over the whole molecule. As shown in Figure S5 by thermal gravimetric analysis and differential scanning calorimetry, dNaAnt sublimates at 368 °C, and the melting point is as high as 355 °C. The good thermal stability paves the way for its application in severe environment.

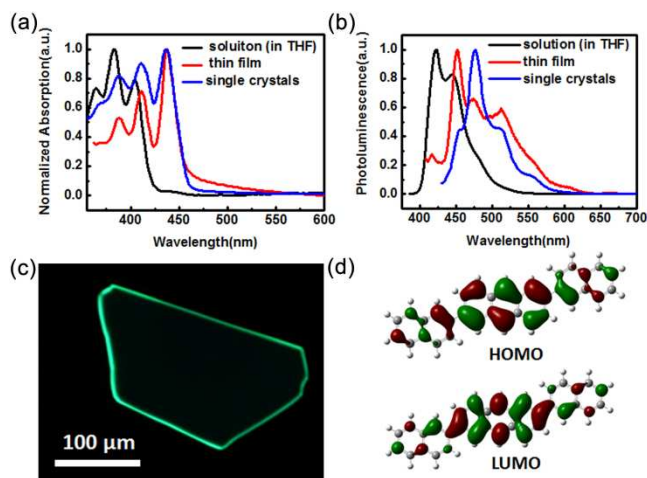


Figure 1. (a, b) UV-vis absorption and photoluminescence spectra of dNaAnt solution (10^{-5} M in THF, black), thin film (red) and single crystals (blue); (c) Fluorescence microscopy of dNaAnt single crystals under UV light; (d) The frontier molecular orbitals of dNaAnt from DFT calculations at the B3LYP/6-31G(d) level.

Using the physical vapor transfer method, the plate-like microcrystals (size: 30 ± 10 μm) were directly grown on the octadecyltrichlorosilane (OTS) modified SiO_2 (300 nm)/Si substrate (Figure 2a, S6). As the deposition time and temperature change, the thickness of the crystals varies from tens of nanometers to hundreds of nanometers, showing obvious step-like layers on the crystal surface (Figure S7). The out-of-plane X-ray diffraction (XRD) patterns of the crystals are shown in Figure 2b, where a series of peaks can be defined as ($h00$). The strong and sharp diffraction peaks indicate the high quality of the crystals. Transmission electron microscopy (TEM) image of an individual crystal and its corresponding selected-area electron diffraction (SAED) pattern are displayed in Figure 2c. The directions $[0k0]$ and $[00l]$ can be assigned with the included angle of 90° . The monoclinic crystal system with lattice constants $a = 23.345$ Å, $b = 7.604$ Å, $c = 5.941$ Å, $\beta = 92.83^\circ$ can be determined using SAED pattern combined with powder XRD pattern and the in-plane XRD, which was indexed in Figure S8. The d -spacing (23.28 Å) calculated from the first order diffraction (3.79°) of out-of-plane XRD is nearly the same as the molecular length (22.61 Å) of dNaAnt via DFT calculation (Figure S9). Same as DPA, the dNaAnt molecule stands almost perpendicularly to the substrate, which is most favorable for charge transport.^{20,21} The regular shape, sharp and strong diffraction peaks, clear and steady diffraction spots imply the superior quality of the dNaAnt crystals.

The “organic ribbon mask” method was applied to build the in situ bottom gate top contact single crystal field-effect transistors (SC-FETs) to evaluate the intrinsic charge transporting property of dNaAnt.²² Typical optical image of an individual device is shown in Figure 2d. Representative transfer and output curves are presented in Figure 2e, 2f. An average mobility of 7.0 $\text{cm}^2 \cdot \text{V}^{-1} \cdot \text{s}^{-1}$ is achieved based on 10 devices (Figure S10a). The mobility for the best device is 12.3 $\text{cm}^2 \cdot \text{V}^{-1} \cdot \text{s}^{-1}$, with a threshold voltage (V_T) around -10 V and an on/off ratio about 3.9×10^7 . It is noteworthy that the device displays not only relatively low threshold voltage but also almost perfect linearity for the $(-I_{\text{DS}})^{1/2} - V_G$ curve, which is rare for ultrahigh mobility (>10 $\text{cm}^2 \cdot \text{V}^{-1} \cdot \text{s}^{-1}$) organic semiconductors. The negligible gate voltage dependence of charge transport for the traditional transistor equations indicates a narrow density of state with few shallow traps in crystal state (Figure S10).^{20,23} The threshold voltage is strongly related to the trap den-

sity at the interface between the dielectric and the semiconductor as revealed by the following equation: $V_T \approx V_{fb} - qN_{tr}/C_i$, where V_{fb} is the flat band voltage, N_{tr} is the trap density, C_i is the dielectric capacitance.²⁴ Since V_{fb} is normally too low to be counted compared with V_T , we can estimate the trap density to be $6.88 \times 10^{11} \text{ cm}^{-2}$ by neglecting the contribution of V_{fb} . In addition, the maximum current of the transfer curve matches well with that of output curve, which is important for practical applications. These characteristics of dNaAnt devices result from the suitable HOMO level, excellent crystal quality and efficient packing structure, which eliminate the traps in the device and facilitate charge transport.

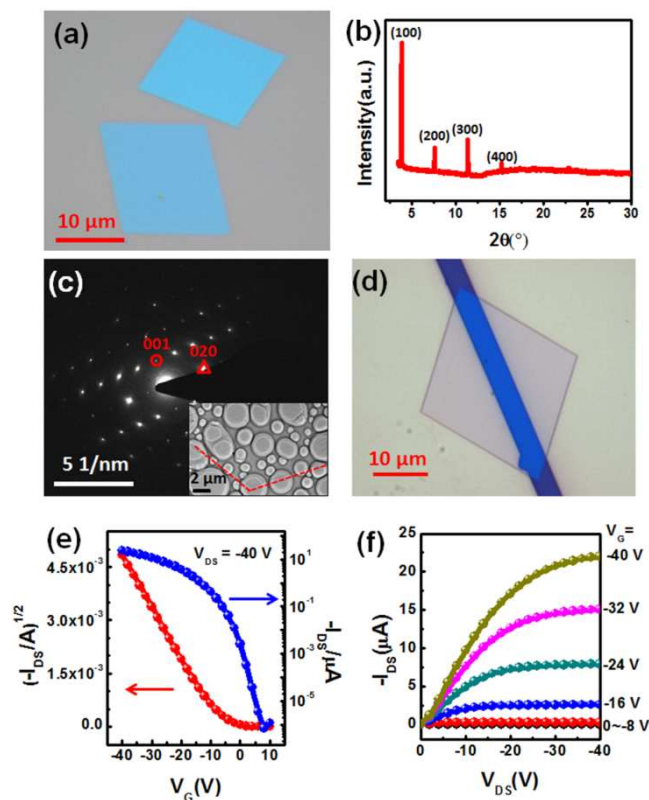


Figure 2. (a) Optical microscopy of dNaAnt micro single crystals; (b) XRD pattern of the single crystals; (c) TEM image of an individual crystal and its corresponding SAED pattern; (d) Optical microscopy of the dNaAnt-based SC-FET device; (e, f) Typical transfer curve and corresponding output curve of a dNaAnt-based SC-FET device.

In view of the excellent electrical and optical property of dNaAnt, light-emitting transistors of dNaAnt single crystals were fabricated with asymmetrical electrodes (Au/MoO₃: Ca/CsF), as shown in Figure 3a, 3b. Owing to the well alignment of the energy levels with the electrodes (Figure 3c), balanced ambipolar charge carrier mobility ($\mu_h = 1.10 \text{ cm}^2 \cdot \text{V}^{-1} \cdot \text{s}^{-1}$, $\mu_e = 0.87 \text{ cm}^2 \cdot \text{V}^{-1} \cdot \text{s}^{-1}$) can be derived from the transfer curve at a relatively low voltage of -60 V or 60 V (Figure 3d), which is one of the best performances for ambipolar OLETs.^{12,25,26} The anisotropy characteristics are displayed in Figure S11, indicating there was no significant difference of the charge transporting property along different packing directions.

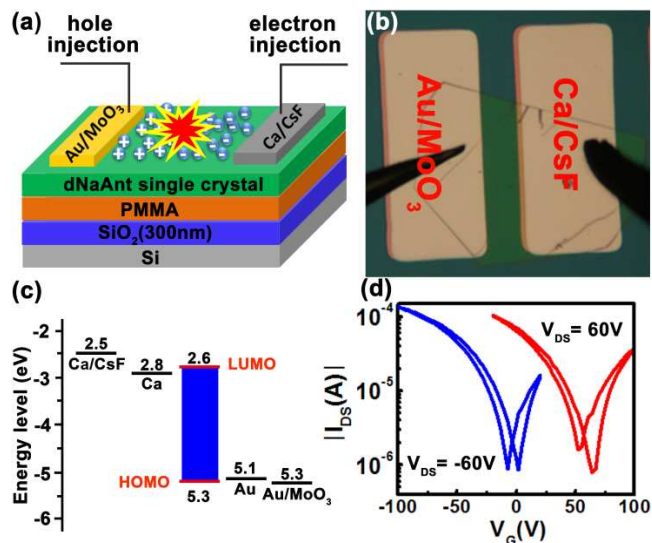


Figure 3. (a, b) Schematic device configuration of the light-emitting transistors; (b) Optical microscopy of the organic light-emitting transistors; (c) Energy level alignment for efficient charge injection; (d) Typical ambipolar transfer curves of the organic light-emitting transistors.

Though the electroluminescence (EL) spectrum is much more resolved with increased intensity in the low energy bands (Figure 4a), the main peaks (452 nm, 474 nm, 516 nm) are almost the same as that of the PL (452 nm, 476 nm, 512 nm). Figure 4b shows the images of the EL with drain-source bias kept constant and the gate voltage being swept. When the drain-source bias is fixed at -60 V, much more negative than the initiated gate voltage (20 V), electrons dominate in the channel. As the gate voltage become more negative, the hole injection starts and the emission was observed at the hole injecting electrode (Au). When the gate voltage is further decreased, the emission zone moves across the channel towards the electron injecting electrode (Ca/CsF). While positive drain-source voltage (60 V) is applied, similar movement of the emission towards the hole injection electrode can be clearly observed (Figure 4c). These characteristics evidenced the ambipolar working mode of the device, which may lead to higher external quantum efficiency than unipolar light-emitting transistors and is believed to be more useful in practical applications.

In conclusion, the introduction of a naphthyl group into the 2,6-sites of the anthracene core indeed allows the following features: (i) prolonged conjugation length and compact packing; (ii) J-aggregated mode; (iii) well alignment of the energy levels with the electrodes. Thus, dNaAnt crystals integrate high mobility ($\mu_{sc} = 12.3 \text{ cm}^2 \cdot \text{V}^{-1} \cdot \text{s}^{-1}$) with efficient solid state luminescence (PLQY = 29.2%). Furthermore, light-emitting transistors of dNaAnt show almost balanced ambipolarity ($\mu_h = 1.10 \text{ cm}^2 \cdot \text{V}^{-1} \cdot \text{s}^{-1}$, $\mu_e = 0.87 \text{ cm}^2 \cdot \text{V}^{-1} \cdot \text{s}^{-1}$) and conspicuous emission can be observed, proving to be one of the best behaviors for ambipolar OLETs. These results make dNaAnt an excellent candidate for integrated optoelectronic applications and offer a facile strategy to the effective combination of excellent charge transporting and efficient solid state emission.

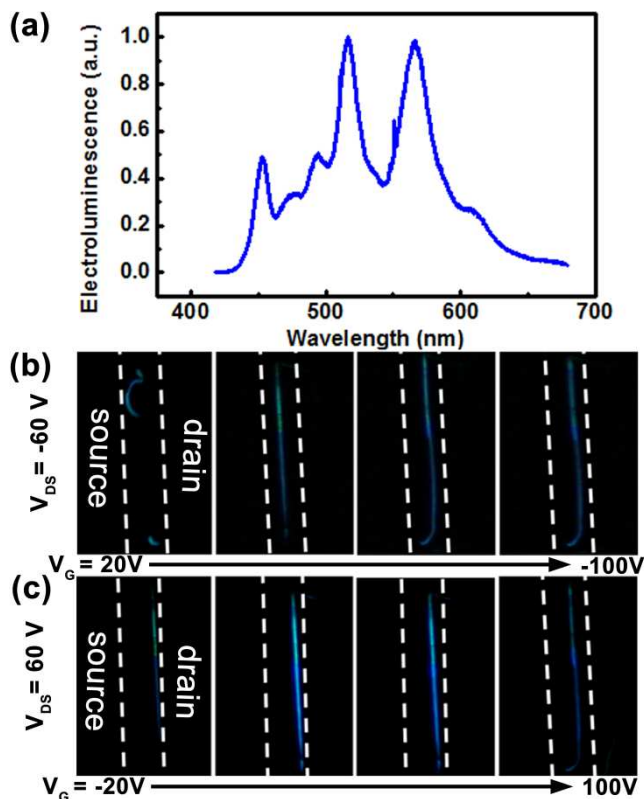


Figure 4 (a) Electroluminescence spectrum (EL) of dNaAnt single crystal; (b, c) Shift of the emission zone within the device channel by tuning the gate voltage.

ASSOCIATED CONTENT

Supporting Information

Experimental details, synthesis, characterization, device fabrication, and theoretical studies. This material is available free of charge via the Internet at <http://pubs.acs.org>.

AUTHOR INFORMATION

Corresponding Author

*zhenyg@iccas.ac.cn

*dhl522@iccas.ac.cn

*huwp@tju.edu.cn

Author Contributions

#J.L., K.Z.: These authors contributed equally to this work.

Notes

The authors declare no competing financial interests.

ACKNOWLEDGMENT

We thank Dr. Yang Li and Mr Jinyu Liu for the calculations and Mr Qiang Zhao for drawing figures. The authors acknowledge the Shanghai Synchrotron Radiation Facility (BL17U1) for the XRD measurements. We are grateful for the financial support from the Ministry of Science and Technology of China (Grants 2016YFB0401100, 2017YFA0204503 and 2015CB856502), the National Natural Science Foundation of China (51733004, 91433115, 51633006, 21661132006, 21473222), the Strategic Priority Research Program (Grant No. XDB12000000) and the Youth Innovation Promotion Association of the Chinese Academy of Sciences.

REFERENCES

- (1) Melzer, C.; von Seggern, H. *Nat. Mater.* **2010**, *9*, 470.
- (2) Muccini, M. *Nat. Mater.* **2006**, *5*, 605.
- (3) Zaumseil, J.; Friend, R. H.; Sirringhaus, H. *Nat. Mater.* **2005**, *5*, 69.
- (4) Cicoira, F.; Santato, C. *Adv. Funct. Mater.* **2007**, *17*, 3421.
- (5) Zaumseil, J.; Sirringhaus, H. *Chem. Rev.* **2007**, *107*, 1296.
- (6) Tessler, N.; Pinner, D. J.; Cleave, V.; Ho, P. K. H.; Friend, R. H.; Yahioglu, G.; Le Barny, P.; Gray, J.; de Souza, M.; Rumbles, G. *Synth. Met.* **2000**, *115*, 57.
- (7) Sundar, V. C.; Zaumseil, J.; Podzorov, V.; Menard, E.; Willett, R. L.; T. Someya, T.; Gershenson, M. E.; Rogers, J. A. *Science* **2004**, *303*, 1644.
- (8) Dadvand, A.; Moiseev, A. G.; Sawabe, K.; Sun, W. H.; Djukic, B.; Chung, I.; Takenobu, T.; Rosei, F.; Perepichka, D. F. *Angew. Chem. Int. Ed.* **2012**, *51*, 3837.
- (9) Dinelli, F.; Capelli, R.; Loi, M. A.; Murgia, M.; Muccini, M.; Facchetti, A.; Marks, T. J. *Adv. Mater.* **2006**, *18*, 1416.
- (10) Ju, H.; Wang, K.; Zhang, J.; Geng, H.; Liu, Z.; Zhang, G.; Zhao, Y.; Zhang, D. *Chem. Mater.* **2017**, *29*, 3580.
- (11) Liu, J.; Zhang, H.; Dong, H.; Meng, L.; Jiang, L.; Jiang, L.; Wang, Y.; Yu, J.; Sun, Y.; Hu, W.; Heeger, A. J. *Nat. Commun.* **2015**, *6*, 10032.
- (12) Bisri, S. Z.; Takenobu, T.; Yomogita, Y.; Shimotani, H.; Yamao, T.; Hotta, S.; Iwasa, Y. *Adv. Funct. Mater.* **2009**, *19*, 1728.
- (13) Melucci, M.; Favaretto, L.; Zambianchi, M.; Durso, M.; Gazzano, M.; Zanelli, A.; Monari, M.; Lobello, M. G.; De Angelis, F.; Biondo, V.; Generali, G.; Troisi, S.; Koopman, W.; Toffanin, S.; Capelli, R.; Muccini, M. *Chem. Mater.* **2013**, *25*, 668.
- (14) Hepp, A.; Heil, H.; Weise, W.; Ahles, M.; Schmechel, R.; von Seggern, H. *Phys. Rev. Lett.* **2003**, *91*, 157406.
- (15) Hsu, B. B.; Duan, C.; Namdas, E. B.; Gutacker, A.; Yuen, J. D.; Huang, F.; Cao, Y.; Bazan, G. C.; Samuel, I. D.; Heeger, A. J. *Adv. Mater.* **2012**, *24*, 1171.
- (16) Park, S. K.; Kim, J. H.; Ohto, T.; Yamada, R.; Jones, A. O. F.; Whang, D. R.; Cho, I.; Oh, S.; Hong, S. H.; Kwon, J. E.; Kim, J. H.; Olivier, Y.; Fischer, R.; Resel, R.; Gierschner, J.; Tada, H.; Park, S. Y. *Adv. Mater.* **2017**, *29*, 1701346.
- (17) Takahashi, T.; Takenobu, T.; Takeya, J.; Iwasa, Y. *Appl. Phys. Lett.* **2006**, *88*, 033505.
- (18) Spano, F. C. *Acc. Chem. Res.* **2010**, *43*, 429.
- (19) Cornil, J.; Beljonne, D.; Calbert, J. P.; Bredas, J. L. *Adv. Mater.* **2001**, *13*, 1053.
- (20) Sirringhaus, H. *Adv. Mater.* **2014**, *26*, 1319.
- (21) Mei, J.; Diao, Y.; Appleton, A. L.; Fang, L.; Bao, Z. *J. Am. Chem. Soc.* **2013**, *135*, 6724.
- (22) Jiang, L.; Gao, J.; Wang, E.; Li, H. X.; Wang, Z. H.; Hu, W.; Jiang, L. *Adv. Mater.* **2008**, *20*, 2735.
- (23) Uemura, T.; Rolin, C.; Ke, T. H.; Fesenko, P.; Genoe, J.; Heremans, P.; Takeya, J. *Adv. Mater.* **2016**, *28*, 151.
- (24) Yoon, M. H.; Kim, C.; Facchetti, A.; Marks, T. J. *J. Am. Chem. Soc.* **2006**, *128*, 12851.
- (25) Takahashi, T.; Takenobu, T.; Takeya, J.; Iwasa, Y. *Adv. Funct. Mater.* **2007**, *17*, 1623.
- (26) Gwinner, M. C.; Kabra, D.; Roberts, M.; Brenner, T. J.; Wallikewitz, B. H.; McNeill, C. R.; Friend, R. H.; Sirringhaus, H. *Adv. Mater.* **2012**, *24*, 2728.

1
2
3
4
5
6
7
8
9
10
11
12
13
14
15
16
17
18
19
20
21
22
23
24
25
26
27
28
29
30
31
32
33
34
35
36
37
38
39
40
41
42
43
44
45
46
47
48
49
50
51
52
53
54
55
56
57
58
59
60

